2018-01-1003 Published 03 Apr 2018

A Novel Three-Planetary-Gear Power-Split Hybrid Powertrain for Tracked Vehicles

Zhaobo Qin, Yugong Luo, Zhong Cao, and Keqiang Li Tsinghua University

Citation: Qin, Z., Luo, Y., Cao, Z., and Li, K., "A Novel Three-Planetary-Gear Power-Split Hybrid Powertrain for Tracked Vehicles," SAE Technical Paper 2018-01-1003, 2018, doi:10.4271/2018-01-1003.

Abstract

Tracked vehicles are widely used for agriculture, construction and many other areas. Due to high emissions, hybrid electric driveline has been applied to tracked vehicles. The hybrid powertrain design for the tracked vehicle has been researched for years. Different from wheeled vehicles, the tracked vehicle not only requires high mobility while straight driving, but also pursues strong steering performance. The paper takes the hybrid track-type dozers (TTDs) as an example and proposes an optimal design of a novel power-split powertrain for TTDs. The commercial hybrid TTD usually adopts the series hybrid powertrain, and sometimes with an extra steering mechanism, which has led to low efficiency and made the structure more complicated. The proposed three-planetary-gear power-split hybrid powertrain can overcome the problems above by utilizing the characteristics of planetary gear sets. The proposed powertrain has two outputs connected to the left and right track respectively, which can provide the accurate torque to both sides of tracks when straight driving, skid steering, or driving backwards. The paper gives the dynamic characteristic matrices to search the big pool of designs with three planetary gear sets more simple. An analytically-based method is used to classify the feasible modes into three groups which have superior dynamic features respectively. Dual-mode designs with two clutches are presented using mode-combination method. A near-optimal control rapid strategy, power-weighted efficiency analysis for rapid sizing (PEARS+), is used as the control strategy. The control results show that the novel design has better drivability and fuel economy than the series hybrid benchmark. The proposed new kind of powertrain has shown good potential which can be considered for future industrial application.

Introduction

Tracked vehicles have been widely used as construction machinery. The emissions, however, can be much higher than those of passenger cars [1]. Moreover, conventional tracked vehicles are also uneconomical, which consumes a great deal of fuel. Thus, hybrid electric tracked vehicles have appeared in the market since 2007. SANY, Kobelco and other companies developed hybrid tracked vehicles one after another. Among them, Caterpillar D7E is the most representative track-type dozer (TTD), which has more than 20% improvement in fuel economy [2]. Due to the improved fuel economy and emissions, hybrid electric technologies are recommended for future tracked vehicles.

Series hybrid, parallel hybrid and power-split hybrid are three main types of hybrid vehicles. For hybrid tracked vehicles, research based on these three types of hybrid are conducted. Series hybrid, however, is the most popular which has been widely commercialized. There are also lots of studies focusing on the energy management, parameter sizing of series hybrid tracked vehicles [3]. Zhang presented a representative operation cycle for series hybrid TTDs which can be used for optimization [4]. Wang proposed a MPC-based energy management strategy for real-time application [5]. Parallel hybrid tracked vehicles can also be found in the market. The research, however, rarely mentioned parallel hybrid as the efficiency at low speed can be hardly improved. Power-split hybrid is usually considered as the most fuel-effective type. Schmitt first invented a power-split hybrid powertrain for tracked vehicles. The powertrain had two modes for low speed and high speed driving. The powertrain, however, had an extra steering motor which made the structure more complicated [6]. This is also the reason why power-split hybrid has not been commercialized. Tracked vehicles need to realize skid steering. Series hybrid can steer using the driving motors without using extra steering mechanism, while current power-split hybrid has to use an extra steering motor. Series hybrid, however, has low energy efficiency relatively.

What if the power-split hybrid tracked vehicle can steer without steering mechanisms? Then the overall efficiency can be guaranteed as well. Thus, the paper proposes a novel hybrid design with three planetary gears (PGs). The design for tracked vehicles has two outputs connected with left and right tracks respectively. This ensures independent control of two sides of tracks while straight driving and skid steering. Moreover, compared with the current series hybrid powertrain, the novel design can be much more efficient.

In effect, power-split hybrid using PGs has been widely researched for wheeled vehicles. Since there can be many connection methods between components and nodes in PGs, many research tended to find the optimal design among the large candidate pool. Liu first proposed the automated modeling method for 2PGs [7], and then Zhang enhanced the

modeling method by adding clutches and brakes [8]. The aforementioned studies both adopted automated modelling method for exhaustive search. Bayrak first proposed another searching method using bond graphs [9]. By establishing bond graphs of all candidates, the method can also identify a near-optimal design rapidly. Silvas enhanced the bond graph based method by solving a constrained logic programming problem [10]. All these methods, however, have not been used for 3PG system and for tracked vehicles.

The novel design proposed in this paper is a 3PG based powertrain, which also need a method to determine the connections between components and modes. Zhuang used to search the design with 3PGs. The total number of candidate designs, however, expands which cannot be searched exhaustively [11]. Thus, an approximate method is used via mode combination. This method, however, can only be applied for one-output system and many assumptions have to be made first. In order to conduct a method which can solve the problem of optimizing multi-output PG system, the paper proposes a specific method which can find the superior designs rapidly.

Control strategy is also important while solving our optimization problem. As fuel economy is an important index of judging tremendous candidate designs, the control strategy has to be previse and time-saving as well. Dynamic programming (DP) can obtain global optimal results, but it has the problem of curse of dimensionality [7]. Equivalent consumption minimization strategy (ECMS) could achieve near-optimal results much faster, but the conversion coefficient has to be changed for different designs [12]. The paper uses power-weighted efficiency analysis for rapid sizing method (PEARS+) in [8] as our control strategy, as it can solve the multi-mode control problems rapidly and achieve near-optimal results compared with DP.

This article first introduces the novel 3PG-based hybrid powertrain for tracked dozers. Then, an optimization method via mode combination is also proposed to find superior design rapidly. Track-type dozer (TTD) is selected as an example in case studies. The proposed powertrain is verified by simulation in Matlab/Simulink. Also, the performances are compared with the current series hybrid benchmark, which can show the promising application of the novel powertrain design.

The Novel Hybrid Powertrain for TTDs

The novel hybrid powertrain has one engine, three motors and two outputs connected to a 3PG set, which is shown in Fig. 1. The two outputs which are connected to two sides of tracks, can be controlled respectively. Not only straight driving, but also turning can be realized by providing traction torques to two outputs independently. The system must have at least two degree of freedom (DOF) to control the two outputs, 3DOF is recommended as the engine can operate with high efficiency.

The novel powertrain can have multi modes by adding clutches and brakes, which can ensure the overall efficiency and improve fuel economy. Moreover, skid steering can be realized without extra steering mechanism.

FIGURE 1 Schematic diagram of the proposed powertrain

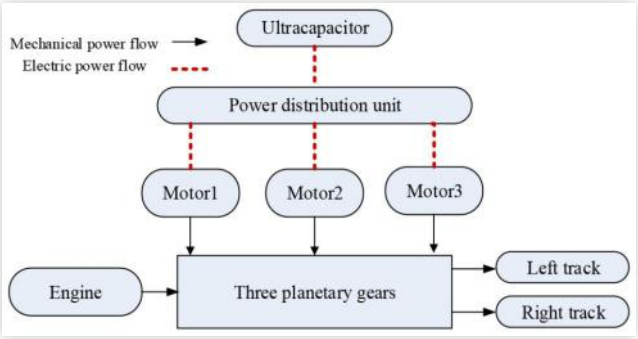

In order to show the advantages of the novel powertrain, a series hybrid TTD is selected as the benchmark. The schematic diagram of the series hybrid TTD benchmark is shown in Figure 2. It has one engine, one generator and two driving motors. The main parameters are shown in Table. 1 [13]. The initial parameters of the novel TTD, engine and ultracapacitor pack are the same as the series benchmark, and three motors in our powertrain has the same size with the driving motors in the series TTD.

The components can be connected with the nine nods in 3PGs, and nodes can also be connected with each other by permanent connection or clutch. Figure 3 shows an example of a multi-mode design and a single mode. MG represents the motor. R, S and C are the ring, sun and carrier gear of a single PG.

FIGURE 2 Schematic diagram of the proposed powertrain

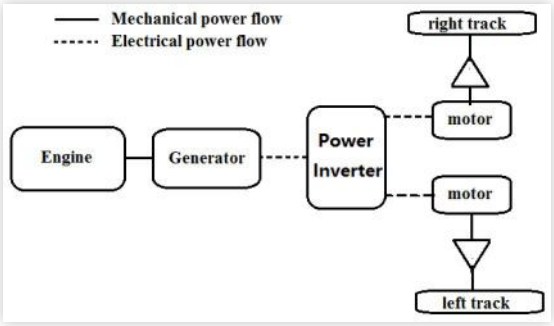

TABLE 1 Key parameters of the benchmark TTD

	Parameter	Value
Vehicle	Vehicle mass (kg)	28,000
	Track length (m)	3.05
	Track gauge (m)	1.786
Diesel Engine	Rated speed (r/min)	1,700
	Rated power (kW)	175
Generator	Max. power (kW)	180
	Max. rotational speed (r/min)	2,200
Motors	Rated Power (kW)	75
	Max. rotational speed (rpm)	6,000
Ultracapacitor	Capacity (F)	2.4
	Voltage (V)	600

FIGURE 3 Example of a candidate design and a mode

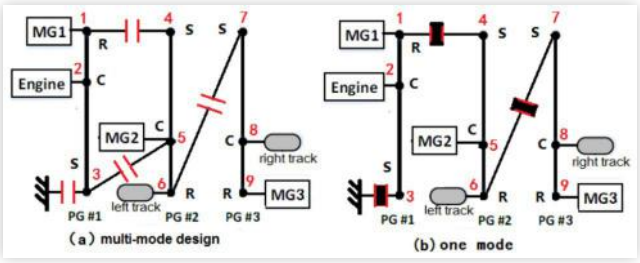

FIGURE 4 Configuration for the case study

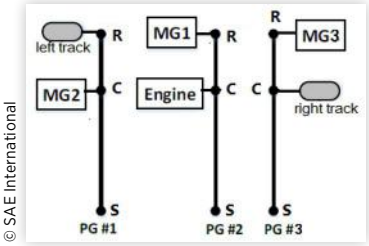

All nine nodes have been tagged from "1" to "9" in order to explain the connections between nodes. The connection vector is defined for a single mode in Fig. 2(b) as in Eq. (1).

$$X_{vector} = \begin{bmatrix} 14 & 30 & 67 \end{bmatrix} \tag{1}$$

"14" means that node 1 and node 4 are connected and "30" means that node 3 is connected with the brake. In this way, all kinds of nodes can be expressed using connection vector. In [11], we can know that there can be a tremendous number of candidate designs using 3PGs. For our novel powertrain, there can be $P_9^6 = 60480$ connection configurations when six components are connected to nine nodes. Moreover, there can be $C_{36}^4 + C_{36}^3 = 3.56 \times 10^9$ modes which has 2DOF or 3DOF. The total number of candidate modes is $P_9^6\left(C_{36}^3 + C_{36}^4\right)$. Thus, exhaustive searching is impossible. We adopt one superior configuration in [14] shown in Fig. 4 and use a design generation method via mode combination to find the near-optimal results rapidly. It should be noted that only switching the PG order or switching the MG number results in the same configuration or design. Details will be shown in the following sections.

Powertrain Model

The vehicle dynamics must be determined before analyzing the detailed performance. The straight driving and skid steering speeds and torques can be calculated referring to [15, 16]. The component model and topology model of PG sets are shown below.

Engine, Motor and Ultracapacitor Model

A static diesel engine map formed by experimental data is used to show the relationship of fuel rate, engine speed and torque. The maximum torques under different rotating speeds are also given as the constraints. The static motor map is also formed by experiments, which shows the relationship of motor speed, torque and efficiency. The engine and motor maps are shown in Fig. 5.

FIGURE 5 Diesel engine and motor map

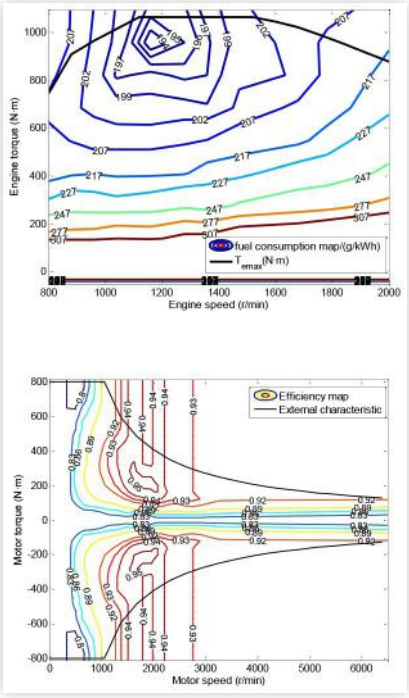

The ultracapacitor pack has nearly 20 modules in series and parallel. In our model, we use a resistance-capacitor circuit to simulate the state of charge (SOC) of the ultracapacitor pack. The limits of SOC is set between 0.1 and 0.9.

Topology Automated Model With the component models given, the dynamics of planetary gears has to be known in order to determine the relationship of the component speed and torque. Analyzing the dynamics of each mode respectively will be time consuming. An automated modeling method is proposed here which can generate the dynamics equations rapidly.

For the design in Fig. 2(a), considering the dynamics of each node, the dynamics relationship in Eq. (2) can be obtained.

$$\begin{bmatrix}
I_e+I_{r2} & 0 & 0 & 0 & 0 & 0 & 0 & 0 & 0 & 0 & -R_2 & 0 \\
0 & I_{V_l}+I_{r1} & 0 & 0 & 0 & 0 & 0 & 0 & 0 & R_1+S_1 & 0 & 0 \\
0 & 0 & I_{V_r}+I_{r3} & 0 & 0 & 0 & 0 & 0 & 0 & 0 & 0 & R_3+S_3 \\
0 & 0 & 0 & I_{mg1}+I_{c2} & 0 & 0 & 0 & 0 & 0 & 0 & R_2+S_2 & 0 \\
0 & 0 & 0 & 0 & I_{mg2}+I_{r1} & 0 & 0 & 0 & 0 & -R_1 & 0 & 0 \\
0 & 0 & 0 & 0 & 0 & I_{mg3}+I_{r3} & 0 & 0 & 0 & 0 & 0 & -R_3 \\
0 & 0 & 0 & 0 & 0 & 0 & I_{s1} & 0 & 0 & -S_1 & 0 & 0 \\
0 & 0 & 0 & 0 & 0 & 0 & 0 & I_{s2} & 0 & 0 & -S_2 & 0 \\
0 & 0 & 0 & 0 & 0 & 0 & 0 & 0 & I_{s3} & 0 & 0 & -S_3 \\
0 & R_1+S_1 & 0 & 0 & -R_1 & 0 & -S_1 & 0 & 0 & 0 & 0 & 0 \\
-R_2 & 0 & 0 & R_2+S_2 & 0 & 0 & 0 & -S_2 & 0 & 0 & 0 & 0 \\
0 & 0 & R_3+S_3 & 0 & 0 & -R_3 & 0 & 0 & -S_3 & 0 & 0 & 0
\end{bmatrix}
\begin{bmatrix} \dot{\omega}_e \\ \dot{\omega}_{V_l} \\ \dot{\omega}_{V_r} \\ \dot{\omega}_{mg1} \\ \dot{\omega}_{mg2} \\ \dot{\omega}_{mg3} \\ \dot{\omega}_{sp1} \\ \dot{\omega}_{sp2} \\ \dot{\omega}_{sp3} \\ F_1 \\ F_2 \\ F_3 \end{bmatrix}
=
\begin{bmatrix} T_e \\ T_{V_l} \\ T_{V_r} \\ T_{mg1} \\ T_{mg2} \\ T_{mg3} \\ 0 \\ 0 \\ 0 \\ 0 \\ 0 \\ 0 \end{bmatrix} \tag{2}$$

where R_i and S_i are the radii of the ring gear and sun gear of the ith PG set. I_e, I_{v_l}, I_{v_r}, I_{mg1}, I_{mg2} and I_{mg3} represent the rotational inertia of the engine, left output, right output and motors. T and $\dot{\omega}$ represent the torque and angular

acceleration of the components. F_1, F_2, and F_3 represent the internal force of the three PG sets. If further divide Eq. (2) into Eq. (3), the J matrix can be defined as inertial matrix $\dot{\Omega}$, T, and F are called speed, torque and internal force matrices. D reflects the component and node connections [7]. When a mode is generated with confirmed connections between nodes as in Fig. 2(b), the dynamics equation will change into Eq. (4).

$$\begin{bmatrix} J & D \\ D^T & 0 \end{bmatrix} \begin{bmatrix} \dot{\Omega} \\ F \end{bmatrix} = \begin{bmatrix} T \\ 0 \end{bmatrix} \tag{3}$$

$$D^* = N \cdot D, \quad J^* = NJN^T, \quad \Omega^* = N \cdot \Omega, \quad T^* = N \cdot T$$

$$\begin{bmatrix} I_e+I_{r2} & 0 & 0 & 0 & 0 & 0 & 0 & -R_2 & 0 \\ 0 & I_{V\_l}+I_{c1} & 0 & 0 & 0 & 0 & R_1+S_1 & 0 & 0 \\ 0 & 0 & I_{V\_r}+I_{c3} & 0 & 0 & 0 & 0 & 0 & R_3+S_3 \\ 0 & 0 & 0 & I_{mg1}+I_{c2} & 0 & 0 & 0 & R_2+S_2 & 0 \\ 0 & 0 & 0 & 0 & I_{mg2}+I_{r1} & 0 & -R_1 & 0 & 0 \\ 0 & 0 & 0 & 0 & 0 & I_{mg3}+I_{r3}+I_{s1}+I_{s2} & -S_1 & -S_2 & -R_3 \\ 0 & R_1+S_1 & 0 & 0 & -R_1 & -S_1 & 0 & 0 & 0 \\ -R_2 & 0 & 0 & R_2+S_2 & 0 & -S_2 & 0 & 0 & 0 \\ 0 & 0 & R_3+S_3 & 0 & 0 & -R_3 & 0 & 0 & 0 \end{bmatrix} \begin{bmatrix} \dot{\omega}_e \\ \dot{\omega}_{V\_l} \\ \dot{\omega}_{V\_r} \\ \dot{\omega}_{mg1} \\ \dot{\omega}_{mg2} \\ \dot{\omega}_{mg3} \\ F_1 \\ F_2 \\ F_3 \end{bmatrix} = \begin{bmatrix} T_e \\ T_{V\_l} \\ T_{V\_r} \\ T_{mg1} \\ T_{mg2} \\ T_{mg3} \\ 0 \\ 0 \\ 0 \end{bmatrix} \tag{4}$$

N matrix is generated using the following rules: Define a unit matrix $I_{9\times 9}$; if the ath node is connected to the bth node, add the elements of the ath row of I to the bth row, then remove the ath row of I; if the ath node is grounded, then remove the ath row.

Eq. (4) can be further simplified into Eq. (5), which can be much clearer to show the speed and torque relationship between components.

$$\begin{bmatrix} \dot{\omega}_e \\ \dot{\omega}_{V\_l} \\ \dot{\omega}_{V\_r} \\ \dot{\omega}_{mg1} \\ \dot{\omega}_{mg2} \\ \dot{\omega}_{mg3} \end{bmatrix} = \mathrm{A}^* \begin{bmatrix} T_e \\ T_{V\_l} \\ T_{V\_r} \\ T_{mg1} \\ T_{mg2} \\ T_{mg3} \end{bmatrix} \tag{5}$$

Where A* is called the dynamics characteristics matrix, which can represent the dynamics of a determined mode. After several derivations, the characteristics matrix A* can be automated written using Eq. (6) below.

$$A^{*'} = (NQ)^T \left\{ \left[I - J^{*-T} D^* \left(D^{*T} J^{*-1} D^* \right)^{-T} D^{*T} \right] J^{*-1} \right\} (NQ) \tag{6}$$

For the configuration in Fig. 3, 2DOF and 3DOF modes can be obtained after adding three or four connections. Thus, A* of all candidate modes can be rapidly written. Among them, by screening out the redundant modes with the same A* matrix, 26,570 unique modes survive which can be used for performance analysis.

Mode Analysis

Since there are two outputs in the powertrain, previous physical mode classification is hard to apply [7]. For example,

FIGURE 6 A mode with both "input-split" and "compound-split" features

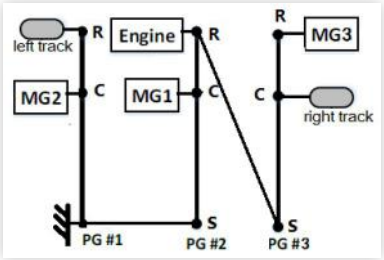

the candidate mode in Fig. 6 can be called "input-split mode" or "compound-split mode" [11]. Thus, in this paper, we classify all modes into three types, namely, feasible attribute mode, superior performance mode, and high overall efficiency mode. Details are shown below.

1. Feasible Attribute (FA) Analysis

For different kinds of tracked vehicles, there can be different attributes. For example, TTD should realize driving backwards with engine-on. Sometimes, central steering should also be guaranteed. The paper takes engine-on backwards as the attribute. Given the characteristic matrices A* of all unique modes, the attributes can be verified directly as shown in Eq. (7).

$$rank\left\{A^*(2:3,:)\right\} = 2, \ \frac{a^*_{21}}{a^*_{22}} > 0, \ \frac{a^*_{31}}{a^*_{33}} > 0 \tag{7}$$

To explain, the second and third rows of A* which represent the output states are written in Eq. (8).

$$\begin{aligned} \frac{\dot{\omega}_{V\_l}}{a^*_{22}} &= \frac{a^*_{21}}{a^*_{22}} T_e + \frac{a^*_{23}}{a^*_{22}} T_{V\_r} + T_{V\_l} + \frac{a^*_{24}}{a^*_{22}} T_{mg1} + \frac{a^*_{25}}{a^*_{22}} T_{mg2} + \frac{a^*_{26}}{a^*_{22}} T_{mg3} \\ \frac{\dot{\omega}_{V\_r}}{a^*_{33}} &= \frac{a^*_{31}}{a^*_{33}} T_e + \frac{a^*_{32}}{a^*_{33}} T_{V\_l} + T_{V\_r} + \frac{a^*_{34}}{a^*_{33}} T_{mg1} + \frac{a^*_{35}}{a^*_{33}} T_{mg2} + \frac{a^*_{36}}{a^*_{33}} T_{mg3} \end{aligned} \tag{8}$$

Since two outputs should be controlled respectively, then $rank\{A^*(2:3,:)\} = 2$ must be satisfied. If the engine can drive the two outputs backwards, then the driven torque must come from the engine. Meanwhile, the engine torque should have different direction from the output torque, which can make the TTD driving backwards. Thus, $\frac{a^*_{21}}{a^*_{22}} > 0, \ \frac{a^*_{31}}{a^*_{33}} > 0$ must be satisfied. The set M_{SP} representing the set of all superior performance modes, is formed as in Eq. (9).

$$M_{FA} = \left\{ m_x \middle| \, A(m_x)^* \in rank\left\{A^*(2:3,:)\right\} = 2, \ \frac{a^*_{21}}{a^*_{22}} > 0, \ \frac{a^*_{31}}{a^*_{33}} > 0 \right\} \tag{9}$$

Among all the 26,570 unique modes, a total number of 7,750 modes survive as feasible attribute modes, the connection vector of these modes are also recorded.

2. Superior Performance (SP) Analysis

The superior performance contains not only the straight driving, but also the turning performance. In this paper, the average maximum traction torque at all speeds is selected as the straight driving index. The average minimum steering radius at all speeds is selected as the turning index shown in Eq. (10).

$$\bar{T}_{\max} = \frac{\sum_{m=1,v_1=0}^{m=k,v_k=v_{\max}} T_{\max}(v_m)}{k}$$
$$\bar{R}_{\min} = \frac{\sum_{n=1,v_1=0}^{n=k,v_k=v_{\max}} R_{\min}(v_n)}{k} \quad (10)$$
$$subject\ to:$$
$$0 \le T_e \le T_{e\_\max}$$
$$0 \le T_{MG} \le T_{MG\_\max}$$
$$0 \le \omega_e \le \omega_{e\_\max}$$
$$-\omega_{MG\_\max} \le \omega_{MG} \le \omega_{MG\_\max}$$

The modes whose average maximum traction torque is higher than the threshold value are designated as straight driving superior performance (SSP) modes. The modes with the average minimum turning radius smaller than the threshold value are designated as turning superior performance (TSP) modes. The set M_{SP} representing the set of all superior performance modes, is formed as in Eq. (11), where $\bar{T}_t$ and $\bar{R}_t$ are the threshold values that represents the average maximum traction torque and minimum turning radius of the series hybrid benchmark.

$$M_{SP} = \left\{ m_x \middle| \bar{T}_{\max}(x) \ge \bar{T}_t \ or\ \bar{R}_{\min}(x) \le \bar{R}_t \right\} \quad (11)$$

The performance of all unique modes are shown in Figure 7, it is shown that 143 unique modes are SSP modes and 724 unique modes are TSP modes. Among them, 121 unique modes are both SSP and TSP modes.

FIGURE 7 Straight driving and turning performance of all modes

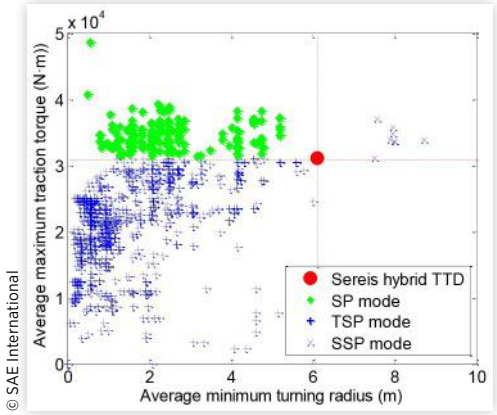

3. High Overall Efficiency (HOE) Analysis

If the engine can operate efficiently by decoupling the engine speed from the output speed, the fuel economy can be improved with high overall efficiency. Thus, parallel modes are not considered here and this part will focus on discussing the efficiency of the power-split modes.

In order to evaluate the overall efficiency, the power flow of a power-split mode is shown in Fig. 8.

P_{ultra}, P_e, and $P_{outputs}$ are the power of the ultracapacitor pack, engine, and outputs. P_{mg} is the motor power which comes from or goes into mechanical flow. P_{MG_elec} is the motor power which comes from or goes into electrical flow. There are two power sources in the powertrain, namely the ultracapacitor pack and the engine. The working conditions of all motors and the engine will influence the overall efficiency. Thus, in this section, the normalized power-weighted efficiency of the motors and engine is introduced for each TTD operating point.

The motors are the only components connected to both the electrical and mechanical path. Thus, there will be energy losses either from the electrical to the mechanical path (driving motor) or from the mechanical to the electrical path (generator). Then the normalized efficiency of the hybrid mode can be shown as in Eq. (12).

$$\eta_{design\_HEV} = \frac{\frac{P_e}{\eta_{e\_\max}} + \frac{\mu P_{uc}\eta_{uc}}{\eta_{uc\_\max}} - \sum_{i=1}^{3} \max\left(\left|P_{mgi\_elec}\right|, \left|P_{mgi\_mech}\right|\right) \cdot \left(1 - \frac{\eta_{mgi}}{\eta_{mgi\_\max}}\right)}{P_{fuel} + \mu P_{uc}} \quad (12)$$
$$\mu = \begin{cases} 0 & P_{uc} \le 0 \\ 1 & P_{uc} > 0 \end{cases}$$

Where $\eta_{uc\_\max}$, $\eta_{e\_\max}$, and $\eta_{mg\_\max}$ are the maximum operating efficiency of the ultracapacitor, engine and motors. Since the engine efficiency is much lower than that of the motor, component power is normalized by their maximum efficiency in order to avoiding using up the ultracapacitor pack. The numerator represents the system "useful" energy, and The denominator represents the total energy consumed. The physical meaning of the proposed efficiency is "the effective availability" of the entire system.

For each vehicle speed and demand torque, different combinations of component speed and torque will lead to

FIGURE 8 Power flow in the powertrain

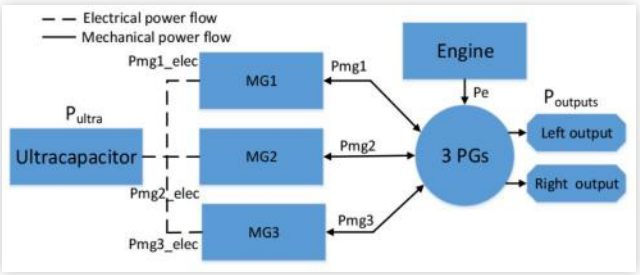

different efficiency. The combination with the maximum efficiency is selected as the best efficiency of this mode as shown in Eq. (13), where v is the vehicle speed and T is the vehicle demand torque.

$$\eta\left(v_x, T_x\right) = \max \eta_{design\_HEV}\left(T_e, T_{mg1}, T_{mg2}, T_{mg3}, \omega_e\right) \tag{13}$$

After proposing the efficiency of each vehicle state, a representative cycle in [4] is used to simulate the overall efficiency of each mode. The cycle is shown in Figure 9. For TTDs, this cycle contains dozing, non-loaded cruising and turning, which reflects the typical working conditions.

The overall efficiency under this cycle can be shown in Eq. (14).

$$\eta_{oveall} = \sum_{n=1,m=1}^{v=v\_\max, T=T\_\max} p\left(v_m, T_n\right)\eta\left(v_m, T_n\right) \tag{14}$$

Where v_m and T_n are all speeds and torques combination, which can cover all working conditions. To avoid repeatedly calculation, $p(v_m, T_n)$ is used to represent the percentage of (v_m, T_n) in the whole driving cycle. The contour map in Fig 10 shows an example normalized efficiency map of the mode in Fig. 6. The blue points are the operating conditions of the representative cycle.

For all candidate modes, the overall efficiency larger than 0.7 is selected as the high overall efficiency (HOE) mode. After the mode analysis as Fig. 10, a total number of 320 modes out of 26,570 survive.

FIGURE 9 Description of the representative cycle of TTDs

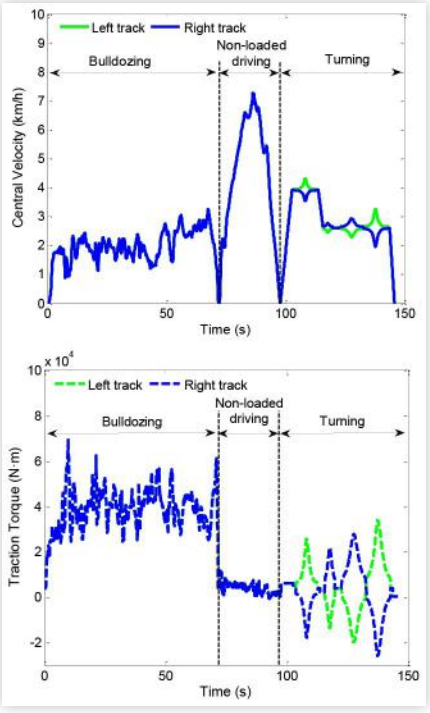

FIGURE 10 An example normalized efficiency map

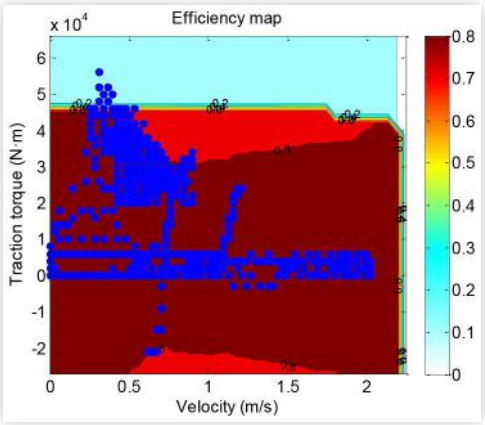

Design Generation via Mode Combination

After mode analysis, all the FA, SP, and HOE modes are obtained. Then combining these three types of modes can generate the designs which can satisfy all requirements of TTDs. In Fig. 2, the connections of all modes have been recorded with the node number of PGs.

Designs with fewer clutches and brakes are more recommended. Thus, the design generation process should try to avoid using too many clutches. In this study, only three clutches and brakes are allowed. Select three modes from FA, SP and HOE groups respectively and combine them together into a candidate design. Assume that the connection vector of one FA mode is X_i^{FA}, the control vector of one SP mode is X_j^{SP}, the control vector of one HOE mode is X_k^{HOE}. Then combine these three modes, and all the connections C_{all}, the clutch position C_{clu}, permanent connection position C_{per} can be represented in Eq. (15).

$$\begin{aligned} C_{all} &= X_i^{FA} \vee X_j^{SP} \vee X_k^{HOE} \\ C_{clu} &= \left(X_i^{FA} \oplus X_j^{SP}\right) \vee \left(X_j^{SP} \oplus X_k^{HOE}\right) \\ C_{per} &= C_{all} \oplus C_{clu} \end{aligned} \tag{15}$$

Since the clutch number should be no more than three, thus Eq. (16) must be satisfied for each generated design. And the designs with clutch number larger than three should be excluded.

$$N_{clutch} = sum\left(C_{clu}\right) =\leq 3 \tag{16}$$

Fig. 11 shows an example of mode combination process by identifying the connection vector. Mode (a) is the FA mode, which is used for driving backwards. Mode (b) is the SP mode which can have better straight driving and turning performance than the series hybrid benchmark. Mode (c) is the HOE mode, which can be fuel-saving. The connection vector of all three modes is shown in Eq. (17), together with the permanent connection and clutch position.

FIGURE 11 An example normalized mode combination process

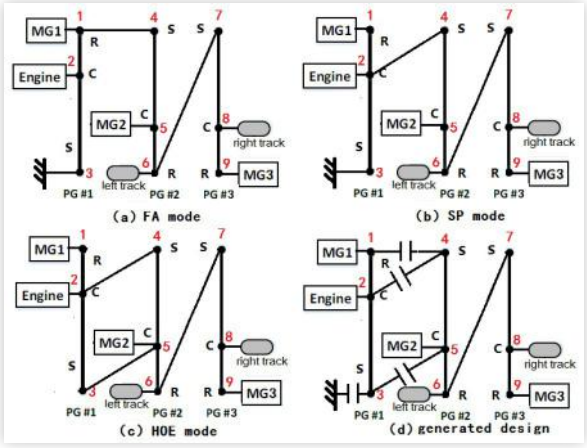

$$
\begin{aligned}
X^a_{vector} &= [14 \;\; 30 \;\; 67] \\
X^b_{vector} &= [24 \;\; 30 \;\; 67] \\
X^c_{vector} &= [24 \;\; 35 \;\; 67] \\
C_{all} &= X^a_{vector} \vee X^b_{vector} \vee X^c_{vector} = [14\ 24\ 30\ 35\ 67] \\
C_{clu} &= \left(X^a_{vector} \oplus X^b_{vector}\right) \vee \left(X^b_{vector} \oplus X^c_{vector}\right) = [14\ 24\ 30\ 35] \\
C_{per} &= C_{all} \oplus C_{clu} = [67]
\end{aligned}
\tag{17}
$$

Thus, although the generated design in Fig 10(d) can satisfy the performance requirements, it has four clutches which will be excluded. After judging all the generated candidate designs, 177 unique designs are left.

Results and Discussion

Fuel economy of these 177 surviving designs is calculated under the typical cycle. PEARS+ is used to obtain the control results rapidly. The procedure of PEARS+ are shown in Fig. 12. There are three main steps. The first and second step has been shown in "mode analysis". In these steps, the component speeds and torques with the maximum normalized efficiency of each mode under all working conditions are calculated first. Then dynamic programming is used to determine the mode shift, which is the low-dimensional problem to ensure the state of charge sustaining. Combine the results of these three steps can have the final near-optimal control executions. Details can be found in [8].

The near-optimal control strategy is applied to all the surviving 177 designs to get the fuel economy results. Then

FIGURE 12 Procedure of the PEARS+ method

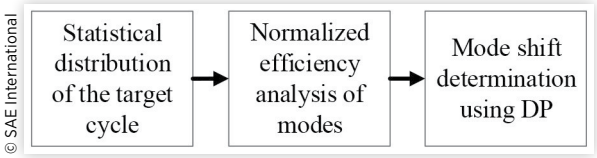

FIGURE 13 The optimal design and the mode chart

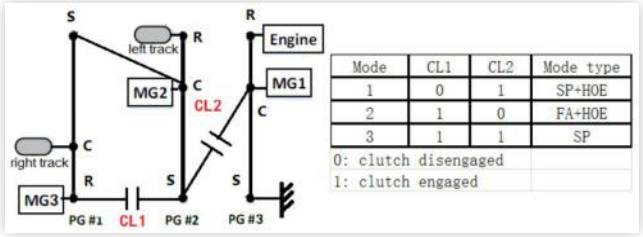

choose the design with the best fuel economy as the final optimal design for this paper. The lever diagram of the optimal design together with its mode chart is shown in Fig. 13.

To further verify the effectiveness of the proposed novel design. The detailed performance comparison is conducted. In Fig. 14, the straight driving and turning performance of the proposed design is compared with the series hybrid benchmark. We can see that the maximum straight driving torque and minimum turning radius are both better than the series hybrid TTD under all speeds.

The control results of the proposed design and the series hybrid benchmark under the typical cycle are shown in Fig. 15. The fuel consumption of the proposed design is 532 g, while that of the series benchmark is 600.9 g. The fuel economy has nearly 11.5% improvement.

FIGURE 14 Straight driving and turning performance comparison

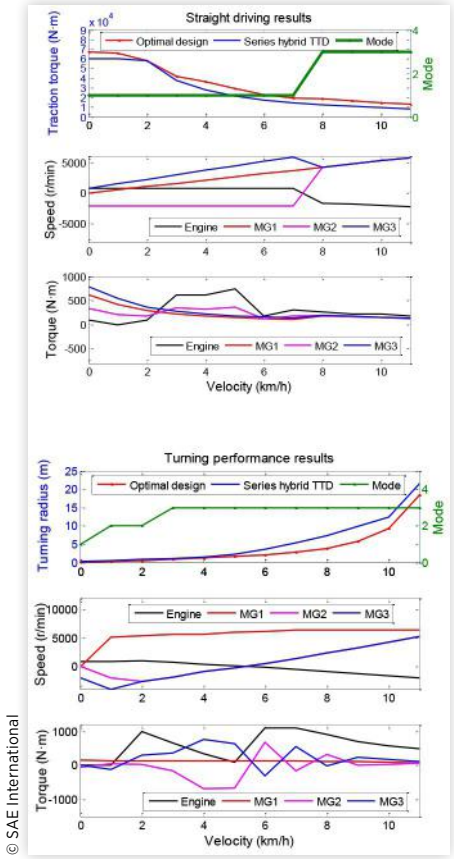

FIGURE 15 State and control trajectories of the series hybrid benchmark and proposed design by PEARS+.

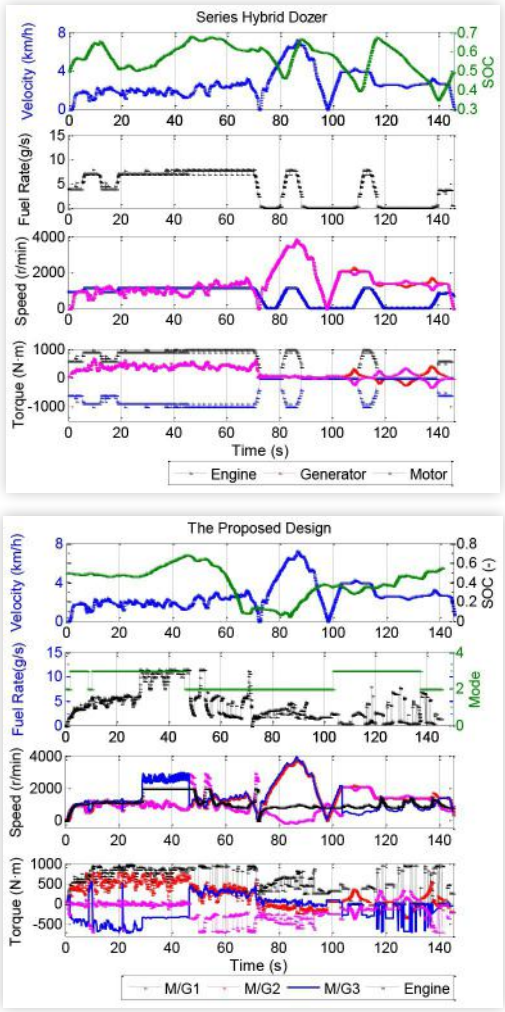

Conclusion

A novel power-split hybrid powertrain using three PGs is presented for hybrid electric tracked vehicles. The powertrain has two outputs connected to two sides of tracks, which can realize engine-on driving backwards, straight driving and skid steering. A design generation method via mode combination is proposed to find the near-optimal design among a great deal of candidate designs rapidly. Modes with feasible attribute, superior performance and high overall efficiency are classified respectively. By combining three modes from these three groups, designs that satisfy the requirements of TTDs can be generated. The case studies show that the generated optimal design can have better performance and better fuel economy than the series hybrid benchmark. The following conclusions can be derived.

1. The novel powertrain can take advantage of the power-split mode to realize high efficiency operating. Moreover, the drivability can be ensured by controlling two sides of tracks respectively without an extra steering mechanism. The novel powertrain has shown promising potential for future industrial use.
2. A near-optimal design generation method via mode combination can be used for powertrain design with multi planetary gears, which can find the required design efficiently instead of exhaustive search.

References

1. Wang, H., Liu, L., Zheng, G., Liu, X. et al., "Study of Two-Motor Hybrid Bulldozer," SAE Technical Paper 2014-01-2376, 2014, doi:10.4271/2014-01-2376.
2. Kwak, S., Kim, T., and Park, G., "Phase-Redundant-Based Reliable Direct AC/AC Converter Drive for Series Hybrid Off-Highway Heavy Electric Vehicles," *IEEE Trans. Veh. Technol.* 59(6):2674-2688, 2010.
3. Zou, Y., Sun, F., Hu, X. et al., "Combined Optimal Sizing and Control for a Hybrid Tracked Vehicle," *Energies* 5(11):4697-4710, 2012.
4. Zhang, Baodi et al. "Development of a Representative Operation Cycle Characterized by Dual Time Series for Bulldozers," *Proceedings of the Institution of Mechanical Engineers, Part D: Journal of Automobile Engineering* (2017): 0954407016687452.
5. Wang, H. et al., "Model Predictive Control-Based Energy Management Strategy for a Series Hybrid Electric Tracked Vehicle," *Applied Energy* 182:105-114, 2016.
6. Schmidt, M.R., "Two-Mode, Compound-Split, Electro-Mechanical, Vehicular Transmission Particulary Adapted for Track-Laying Vehicles," U.S. Patent 6,491,599, 2002-12-10.
7. Liu, J. and Peng, H., "Modeling and Control of a Power-Split Hybrid Vehicle," *IEEE Trans. Contr. Syst. Technol.* 16(6):1242-1251, 2008.
8. Zhang, X., Li, S.E., and Peng, H., "Efficient Exhaustive Search of Power-Split Hybrid Powertrains with Multiple Planetary Gears and Clutches," *Journal of Dynamic Systems, Measurement, and Control* 137(12):121006, 2015.
9. Bayrak, A.E., Ren, Y., and Papalambros, P.Y., "Design of Hybrid-Electric Vehicle Architectures Using Auto-Generation of Feasible Driving Modes," *ASME 2013 International Design Engineering Technical Conferences and Computers and Information in Engineering Conference*, American Society of Mechanical Engineers, 2013, V001T01A005-V001T01A005.
10. Silvas, E., Hofman, T., Serebrenik, A. et al., "Functional and Cost-Based Automatic Generator for Hybrid Vehicles Topologies," *IEEE/ASME Transactions on Mechatronics* 20(4):1561-1572, 2015.
11. Zhuang, W., Zhang, X., Peng, H. et al., "Rapid Configuration Design of Multiple-Planetary-Gear Power-Split Hybrid Powertrain Via Mode Combination," *IEEE/ASME Transactions on Mechatronics* 21(6):2924-2934, 2016.
12. Musardo, C., Rizzoni, G., and Guezennec, Y., "A-ECMS: An Adaptive Algorithm for Hybrid Electric Vehicle Energy Management," *European Journal of Control* 11(4-5):509-524, 2005.

13. Wang, H., Huang, Y., Khajepour, A. et al., "*A Novel Energy Management for Hybrid Off-Road Vehicles without Future Driving Cycles as A Priori*," (Energy, 2017).
14. Qin, Z., Luo, Y., Li, K. et al. "A New Powertrain Design Approach for Power-Split Hybrid Tracked Vehicles," *2017 Dynamic Systems and Control Conference*, American Society of Mechanical Engineers, 2017.
15. Shabana, A.A., "Nonlinear Dynamics of Tracked Vehicles[R]," Chicago Univ IL, 1997.
16. Qin, Z., Luo, Y., Zhuang, W. et al., "Simultaneous Optimization of Topology, Control and Size for Multi-Mode Hybrid Tracked Vehicles," *Applied Energy* 212:1627-1641, 2018.

Contact Information

Zhaobo Qin
Tsinghua University
Beijing, China
qzb13@mails.tsinghua.edu.cn

Yugong Luo
Tsinghua University
Beijing, China
lyg@tsinghua.edu.cn

Zhong Cao
Tsinghua University
Beijing, China
caoc15@mails.tsinghua.edu.cn

Keqiang Li
Tsinghua University
Beijing, China
likq@tsinghua.edu.cn

Acknowledgments

The authors appreciate the financial support of the National Key R&D Program of China (No. 2016YFB0100905) and International Science & Technology Cooperation Program of China under contract No. 2016YFE0102200.

ISSN 0148-7191